ISSN 1064-2269, Journal of Communications Technology and Electronics, 2007, Vol. 52, No. 3, pp. 343–351. © Pleiades Publishing, Inc., 2007.
Original Russian Text © A.A. Koronovskii, R.A. Filatov, A.E. Hramov, 2007, published in Radiotekhnika i Elektronika, 2007, Vol. 52, No. 3, pp. 362–372.

DYNAMIC CHAOS IN RADIOPHYSICS AND ELECTRONICS

Chaotic Synchronization in Distributed Beam–Plasma Systems with Supercritical Current

A. A. Koronovskii, R. A. Filatov, and A. E. Hramov

Received September 12, 2005

Abstract—Chaotic synchronization is found to arise in coupled beam–plasma systems with supercritical current. It is shown that, with increasingly stronger coupling, such systems pass from asynchronous behavior via phase synchronization to complete synchronization. Chaotic synchronization is studied according to a method based on the introduction of a continuous set of phases of the chaotic signal. In the case of unidirectional coupling, a generalized chaotic synchronization mode is observed. The mechanism of its emergence in the beam–plasma systems is investigated via the modified-system method.

PACS numbers: 05.45.Gg, 52.40.Mj

DOI: 10.1134/S1064226907030096

INTRODUCTION

Synchronization of chaotic oscillations in systems of various types is one of the most important directions in the field of radiophysics and nonlinear dynamics [1–3]. Chaotic synchronization modes are observed for a number of coupled physical, chemical, and biological systems [4–6]. Such operating conditions require different approaches to the diagnostics of the corresponding synchronous modes [7–12]. At present, several types of chaotic synchronization have been distinguished: generalized [13], phase [2], and lag synchronization [10]; complete synchronization [14]; and synchronization of time scales [12, 15], which generalizes the types mentioned above [16–18].

Generalized synchronization [13] implies that there exists a certain functional dependence between the states of chaotic oscillators, i.e., that $\vec{x}_2(t) = \vec{F}[\vec{x}_1(t)]$, where $\vec{x}_{1,2}$ are the state vectors of the coupled systems. Phase synchronization [2] means that the phases of chaotic signals are locked, while their amplitudes remain uncoupled and appear to be chaotic. Lag synchronization [10] involves such a mode of combined oscillations in which the dynamics of each of the subsystems is shifted by time τ with respect to the dynamics of the other system: $\vec{x}_1(t) \approx \vec{x}_2(t-\tau)$. Finally, synchronization is called complete [14] if the dynamics of the chaotic oscillators is identical: $\vec{x}_1(t) \approx \vec{x}_2(t)$.

In [12, 15–18], we have shown that generalized, phase, lag, and complete synchronizations are closely related and, in essence, are the manifestations of the same type of synchronous oscillations of coupled oscillators that is referred to as synchronization of time scales. The specific character of a synchronous mode (phase, generalized, lag, or complete synchronization) is determined by the number of synchronized time scales, which are introduced with the help of a continuous wavelet transform [19]. Since time scale s is related to the frequency, synchronization of chaotic oscillations is associated with phase coupling between frequency components ω of Fourier spectra $S(\omega)$ [12, 20].

Most studies devoted to chaotic synchronization have been conducted for systems with a small number of degrees of freedom [1–3, 14] or for reference models of distributed systems (chains and arrays of coupled nonlinear chaotic oscillators [21, 22], the Ginzburg–Landau coupled equations [1, 23], the Kuramoto–Sivashinskii coupled equations [24], etc.). Chaotic synchronization in beam–plasma systems has been studied only meagerly: There are virtually no detailed studies devoted to this phenomenon (with the rare exception of [25]). Transitions between different types of chaotic synchronization have not been studied for such systems, and no comparison with chaotic synchronization in systems with a few degrees of freedom has been accomplished. Investigation of chaotic synchronization in distributed beam–plasma systems of the microwave frequency band seems important in view of the wide range of possibilities this phenomenon offers for the data transmission in chaotic modes [26] and for the control over chaotic oscillations in microwave electronics systems [27, 28].

In this study, we consider chaotic synchronization in coupled beam–plasma systems with supercritical current in terms of the hydrodynamic models of the Pierce diode [29, Lecture 4]. These models are of much help in demonstrating various types of chaotic behavior of plasma systems [29–36].

1. MATHEMATICAL MODEL

A Pierce diode is comprised of two infinite planar parallel grids, which are penetrated by a monoenergetic (at the input) electron flow. The grids bounding the structure are grounded and spaced at distance L from one another. Charge density ρ_0 and electron velocity v_0 in the flow entering the system are kept constant. The intergrid space is filled uniformly with a neutralizing background of quiescent ions. Density $|\rho_i|$ of the neutralizing charge in a classical Pierce diode is equal to unperturbed charge density $|\rho_0|$ in the flow.

The single control parameter of the problem is the Pierce parameter $\alpha = \omega_p L/v_0$, which has the meaning of the unperturbed transit angle in terms of plasma frequency ω_p (v_0 is the velocity of electrons entering the intergrid space and L is the distance between the grids). Such an electron flow traveling through a Pierce diode is the simplest electron–plasma system. As a model of a distributed active medium, this model allows consideration of instabilities that appear in the electron flow and the influence of the boundary conditions on these instabilities [38, 39]. At $\alpha > \pi$, the Pierce instability develops in the system, thus leading to the formation of a virtual cathode and the multiflow state of the beam (for more details, see [29, 30]). However, at $\alpha \sim 3\pi$, the single-flow state of the beam is settled and the system can be described within the framework of hydrodynamic approximation [29, 30, 33]. It is shown in [29–33, 36, 40] that beam–plasma chaotic oscillations of various types are observed in this case.

Let us consider two coupled Pierce diodes, which can be described in the hydrodynamic approximation by a self-consistent system of the equations of motion, the continuity equation, and the Poisson equation that are written for dimensionless variables (for more details, see [29]):

$$\frac{\partial^2 \varphi_{1,2}}{\partial x^2} = \alpha_{1,2}^2(\rho_{1,2} - 1), \tag{1}$$

$$\frac{\partial \rho_{1,2}}{\partial t} = -\frac{\partial(\rho_{1,2} v_{1,2})}{\partial x}, \tag{2}$$

$$\frac{\partial v_{1,2}}{\partial t} = -v\frac{\partial v_{1,2}}{\partial x} - \frac{\partial \varphi_{1,2}}{\partial x}, \tag{3}$$

with the boundary conditions

$$v_{1,2}(0, t) = 1, \quad \rho_{1,2}(0, t) = 1, \quad \varphi_{1,2}(0, t) = 0, \tag{4}$$

where indices 1 and 2 refer to the first and the second coupled beam–plasma system, respectively.

Dimensionless variables of potential φ, density ρ, velocity v of the electron fluid, spatial coordinate x, and time t in Eqs. (1)–(3) relate to the corresponding dimensional variables through the relationships

$$\varphi' = (v_0^2/\eta)\varphi, \quad \rho' = \rho_0\rho,$$
$$v' = v_0 v, \quad x' = Lx, \quad t' = (L/v_0)t, \tag{5}$$

where the primes mark the dimensional quantities, η is the electron charge, and v_0 and ρ_0 are, respectively, the static (unperturbed) velocity and density of the electron fluid.

We consider the cases of two Pierce diodes connected by reciprocal and unidirectional coupling. The bidirectional (reciprocal) coupling was modeled by means of changing the dimensionless potential at the right boundary of both coupled systems,

$$\varphi_{1,2}(x = 1.0, t) = \varepsilon\{\rho_{1,2}(x = 1.0, t) - \rho_{1,2}(x = 1.0, t)\}. \tag{6}$$

In the case of unidirectional coupling, the boundary conditions for the potential are given in the form

$$\varphi_1(1, t) = 0,$$
$$\varphi_2(1, t) = \varepsilon(\rho_1(x = 1, t) - \rho_2(x = 1, t)), \tag{7}$$

where the first (index 1, drive) system is in the self-sustained oscillation mode. This system exerts an influence on the second (index 2, response) system.

In nonstationary boundary conditions describing reciprocal (6) and unidirectional (7) couplings between the systems, quantity ε is the coupling parameter and $\rho_{1,2}(x = 1.0, t)$ are the oscillating dimensionless space-charge densities detected at the output of these systems. Experimentally, the oscillating space-charge density of the electron beam can be detected by a section of a helical slow-down system [41] that is placed at the output of the diode gap formed by the grids [37] that are transparent to the electron flow. Then, the output signal of the slow-down section of the first system is applied to one of the grids of the second system, thus modulating the potential difference in the interaction space. In this case, parameter ε depends on the parameters of both the slow-down system (coupling resistance, the system length, etc.) and the transmission line (impedance, attenuation, etc.).

System of partial differential equations (1)–(3) was numerically integrated via the finite-difference technique [29, Lecture 4]. Continuity equation (2) and equation of motion (3) were solved with a difference scheme in the direction opposite to the flow direction, and Poisson equation (1) was solved through the error-vector propagation method [42]. The main parameters of the numerical scheme, the space and time steps, were chosen to be $\Delta x = 0.005$ and $\Delta t = 0.003$, respectively.

It is known [29] that, in the autonomous hydrodynamic model of a Pierce diode, a decrease in parameter

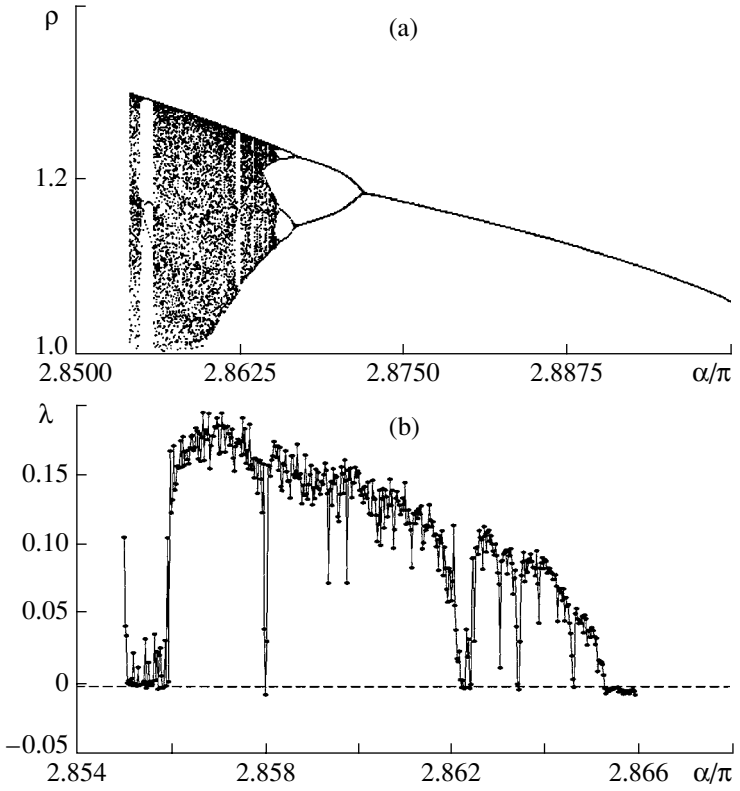

Fig. 1. (a) Bifurcation diagram and (b) the maximum Lyapunov exponent for an autonomous Pierce diode vs. parameter α.

α from 2.850π to 2.870π initiates transition of the space charge to chaotic space–time dynamics via a series of period doublings. This transition is illustrated in Fig. 1, which shows the bifurcation diagram of the space–charge density oscillations at the point $x = 0.2$ of the interaction space and the dependence of the highest Lyapunov exponent on the Pierce parameter. The value of highest Lyapunov exponent λ was calculated with Benettin's algorithm tailored to the analysis of a spatially distributed system. (This technique is detailed in [43].) Figure 1 shows that, with a decrease in Pierce parameter α, the oscillation complexity, which is estimated from the size of the chaotic attractor (Fig. 1a) and positive Lyapunov exponent λ (Fig. 1b), grows on average.

2. COMPLETE SYNCHRONIZATION AND SYNCHRONIZATION OF TIME SCALES IN CHAOTIC DISTRIBUTED SYSTEMS WITH RECIPROCAL COUPLING

Let us investigate the dynamics of Pierce diodes (1)–(3) with reciprocal coupling (6) in the case when the Pierce parameter of one system is constant, $\alpha_1 = 2.861\pi$, and the Pierce parameter of the second system varies in the interval 2.850π to 2.870π, in which the system passes to chaotic dynamics, as was shown above.

Numerical modeling has shown that, at a small detuning $\Delta\alpha = \alpha_1 - \alpha_2$ between the chaotic systems, the mode of time-scale synchronization sets in, as was concluded from the analysis of the phase-difference dynamics on various time scales s. A continuous set of chaotic-signal phases $\varphi_s(t)$ on different time scales s was introduced with the help of a continuous wavelet transform [12, 15–18]. The time series to be analyzed comprised the values of chaotically oscillating space-charge densities $\rho_{1,2}(t)$ taken at the point $x = 0.2$ of the interaction space.

In essence, chaotic synchronization of time scales [12, 15–18] can be represented as follows. Consider a wavelet transform of a certain chaotic signal $\xi(t)$,

$$W(s, t_0) = \int_{-\infty}^{+\infty} \xi(t)\psi^*_{s, t_0}(t)dt, \qquad (8)$$

where $\psi_{s, t_0}(t) = (1/\sqrt{s})\psi_0((t - t_0)/s)$ is the wavelet function stemming from generating wavelet $\psi_0(t)$. Time scale s determines wavelet width $\psi_{s, t_0}(t)$ and t_0 is the time shift of the wavelet function along the time axis (the asterisk denotes complex conjugation) [19]. Note that, for the wavelet transform, the term *time scale* is commonly used instead of the term *frequency*, which is typical of the Fourier transform.

Following [15, 16, 18], we take the parent wavelet in the form of the Morlet wavelet, $\psi_0(\eta) =$

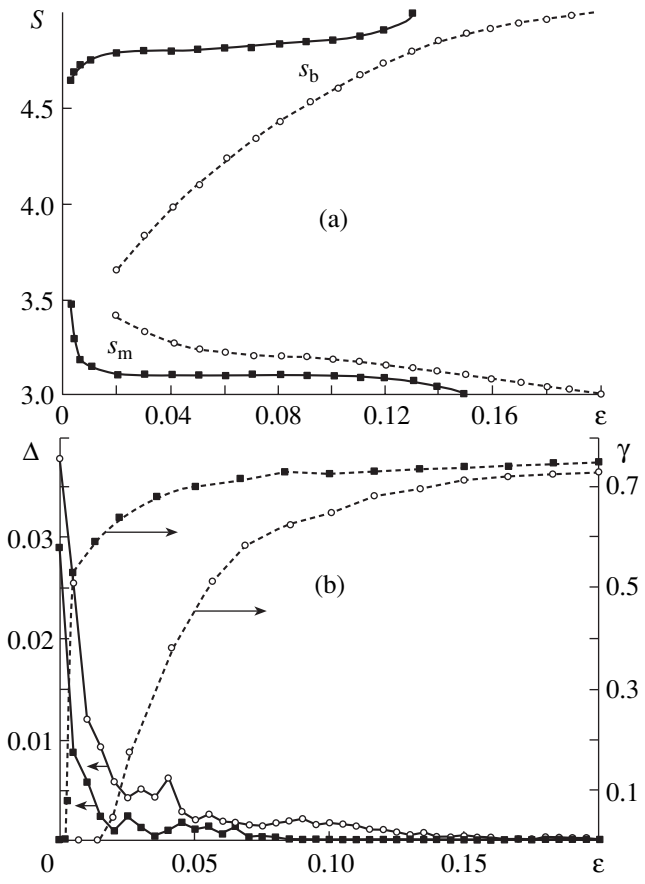

Fig. 2. (a) Lower boundary s_m and upper boundary s_b of the region of synchronized scales and (b) measure of identity of oscillations Δ and fraction of the oscillation energy contained in synchronous scales γ vs. coupling parameter ε for (squares) small ($\alpha_1/\pi = 2.860$, $\alpha_2/\pi = 2.861$) and (circles) large ($\alpha_1/\pi = 2.860$ and $\alpha_2/\pi = 2.858$) detunings of the control parameters.

$(1/\sqrt[4]{\pi})\exp(j\omega_0\eta)\exp(-\eta^2/2)$ [19]. If the wavelet parameter is taken to be $\omega_0 = 2\pi$, time scale s of the wavelet transform is related to frequency f of the Fourier transform as $s = 1/f$.

The wavelet spectrum of signal $\xi(t)$,

$$W(s, t_0) = |W(s, t_0)|\exp[j\phi_s(t_0)] \quad (9)$$

characterizes the behavior of the system on each time scale s at arbitrary time t_0. Absolute value $|W(s, t_0)|$ characterizes the intensity of the corresponding time scale s at time t_0. It is convenient to introduce an integral distribution of the wavelet-spectrum energy with respect to the time scales:

$$\langle E(s)\rangle = \int |W(s, t_0)|^2 dt_0. \quad (10)$$

Then, the wavelet phase is naturally defined as $\phi_s(t) = \arg W(s, t)$ for each time scale s. In other words, it becomes possible to characterize the behavior of each time scale s by associated phase $\phi_s(t)$.

If there exists a certain range of time scales $[s_m, s_b]$ such that the condition of phase locking,

$$|\phi_{s1}(t) - \phi_{s2}(t)| < \text{const} \quad (11)$$

is fulfilled on any time scale $s \in [s_m, s_b]$ and the fraction of wavelet-spectrum energy (10) that falls into this interval is nonzero,

$$E_{snhr} = \int_{s_m}^{s_b} \langle E(s)\rangle ds > 0, \quad (12)$$

then times scales $s \in [s_m, s_b]$ are synchronized and the chaotic generators are in the mode of time-scale synchronization [12, 15–18]. In this case, phases of the first and second systems $\phi_{s1,2}(t)$ appearing in (11) are continuous phases corresponding to synchronized time scales s.

Having introduced a continuous set of time scales s with the associated phases of a chaotic signal and extracted the range of synchronous scales $\Delta s = s_2 - s_1$, we can define a quantitative measure of the chaotic synchronization of coupled systems as the relative contribution of the energy contained in synchronous time scales to the wavelet-spectrum energy,

$$\gamma = \int_{s_m}^{s_b} \langle E(s)\rangle ds \Big/ \int_0^\infty \langle E(s)\rangle ds, \quad (13)$$

where $\langle E(s)\rangle$ is the integral distribution of the wavelet-spectrum energy over the scales, as given by formula (10). If $\gamma = 0$, the mode of time-scale synchronization is absent; if $\gamma \neq 0$, this mode is realized and the synchronized scales are those specified by conditions (11) and (12). If $\gamma = 1$, oscillations in each of the subsystems are close to each other. Such a mode is known as complete synchronization. As energy γ grows from 0 to 1, the fraction of energy contained within synchronous time scales s likewise grows.

Let us proceed with discussing the reciprocal oscillations in terms of the hydrodynamic models of Pierce diodes.

Figure 2a illustrates the behavior of coupled beam–plasma systems at $\alpha_1 = 2.861\pi$ and $\alpha_2 = 2.860\pi$. Limiting synchronous scales s_m and s_b are shown as functions of coupling factor ε. It is seen from Fig. 2a that, at $\varepsilon > 0.0007$, time scales appear on which the dynamics of the beam–plasma oscillations is synchronous. As was mentioned above, this mode corresponds to the time-scale synchronization of chaotic oscillations. As coupling parameter ε grows, the range of synchronous oscillations widens and, at $\varepsilon \approx 0.08$–0.10, synchronous dynamics is observed practically within the entire range

of the time scales: The arising mode is close to synchronization of the subsystems whose oscillations are shifted by time $\tau \approx 0.07$. With a further increase in ε, the time shift between two subsystems diminishes and the system tends toward the complete chaotic synchronization mode, in which oscillations in both coupled subsystems are nearly identical ($\tau \approx 0$).

For a larger detuning $\Delta\alpha$ between the Pierce parameters of the coupled beam–plasma systems, the spectrum of oscillations in the electron beam is substantially more complicated and time-scale synchronization is observed at larger values of the coupling factor. Figure 2a shows boundaries $[s_m, s_b]$ of the region of synchronous scales in the case $\alpha_1 = 2.860\pi$ and $\alpha_2 = 2.858\pi$. As in the case considered above, a range of synchronous time scales emerges at a certain value of coupling parameter ε and the system tends toward the mode of complete chaotic synchronization; however, this process occurs at much higher values of the coupling parameter than in the case of small detuning. To estimate the closeness of space–time chaotic oscillations in each of the distributed systems, we calculated identity measure Δ as a function of ε in the following form [44]:

$$\Delta = \langle |\rho_1(x, t) - \rho_2(x, t)| + |v_1(x, t) - v_2(x, t)| + |\phi_1(x, t) - \phi_2(x, t)| \rangle, \quad (14)$$

where symbol $\langle \ldots \rangle$ denotes the time and space averaging. The results are plotted in Fig. 2b, which shows that function $\Delta(\varepsilon)$ rapidly drops with the growth of coupling and tends toward zero. As seen from Fig. 2b (circles), the value of Δ remain nonzero even at a large detuning between the parameters of the beam–plasma system (although it becomes fairly small at $\varepsilon > 0.17$). This behavior is in contrast to that in the case of a small detuning (Fig. 2b, squares). The oscillation modes in which $\Delta(\varepsilon) \approx 0$ are the modes of complete chaotic synchronization.

As was mentioned above, an important characteristic of the synchronous behavior of coupled chaotic systems is synchronization measure γ (13), which is defined as the relative contribution of the energy in synchronous time scales to the energy of the wavelet spectrum. In Fig. 2b, dependences $\gamma(\varepsilon)$ are plotted for two sets of the control parameters $\alpha_{1,2}$ considered above. It is seen that the growth of the coupling parameter leads to an increase in γ, a circumstance that means that oscillations in each of the distributed systems tend toward identity and, as a result, the complete chaotic synchronization mode is established (at large values of the coupling parameter).

Figure 3 represents plane (α_2, ε) of the control parameters with the plotted boundary of the region of complete chaotic synchronization in a system of reciprocally coupled Pierce diodes for the constant parameter $\alpha_1 = 2.861\pi$. It is seen that, with an increase in the coupling parameter, the complete synchronization mode is observed for any detuning of control parameters $\alpha_{1,2}$. This fact is related both to weakly chaotic oscillations and a small detuning and to well-developed chaos, during which the control parameters of the subsystems are considerably different. The complete synchronization mode is established at a lower value of coupling parameter ε in subsystems with a smaller detuning.

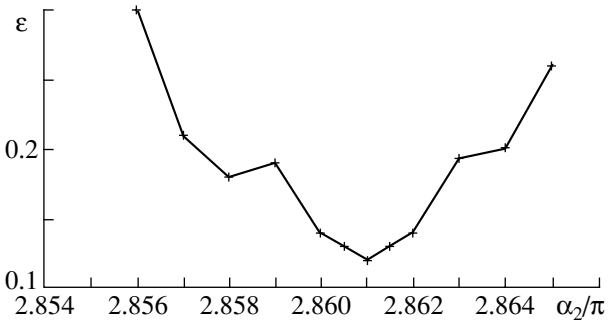

Fig. 3. Boundary of the complete chaotic synchronization mode in the plane of parameters $(\alpha_2/\pi, \varepsilon)$ for $\alpha_1 = 2.861\pi$.

3. GENERALIZED SYNCHRONIZATION IN UNIDIRECTIONALLY COUPLED PIERCE DIODES

We now turn to the phenomenon of generalized synchronization in the coupled systems under study. Generalized synchronization can be introduced for unidirectionally coupled systems only; therefore, we consider chaotic oscillation modes of unidirectional coupling (7) between beam–plasma subsystems with supercritical current.

To identify the generalized synchronization mode, we used the auxiliary system approach [9] and an algorithm for calculation of the maximum conditional Lyapunov exponent [8, 45]. In general outline, the auxiliary system approach can be described as follows. Along with response system $\vec{x}_r(t)$, auxiliary system $\vec{x}_a(t)$ identical to the response system is considered. Initial conditions for auxiliary system $\vec{x}_a(t_0)$ are chosen to be different from those of response system $\vec{x}_r(t_0)$. In the absence of generalized synchronization, the state vectors of response system $\vec{x}_r(t)$ and of auxiliary system $\vec{x}_a(t)$ belong to the same chaotic attractor but differ from each other. In the generalized synchronization mode, by force of the relationship $\vec{x}_r(t) = \vec{F}[\vec{x}_d(t)]$ and, therefore, of the relationship $\vec{x}_a(t) = \vec{F}[\vec{x}_d(t)]$, the states of the response and auxiliary systems must

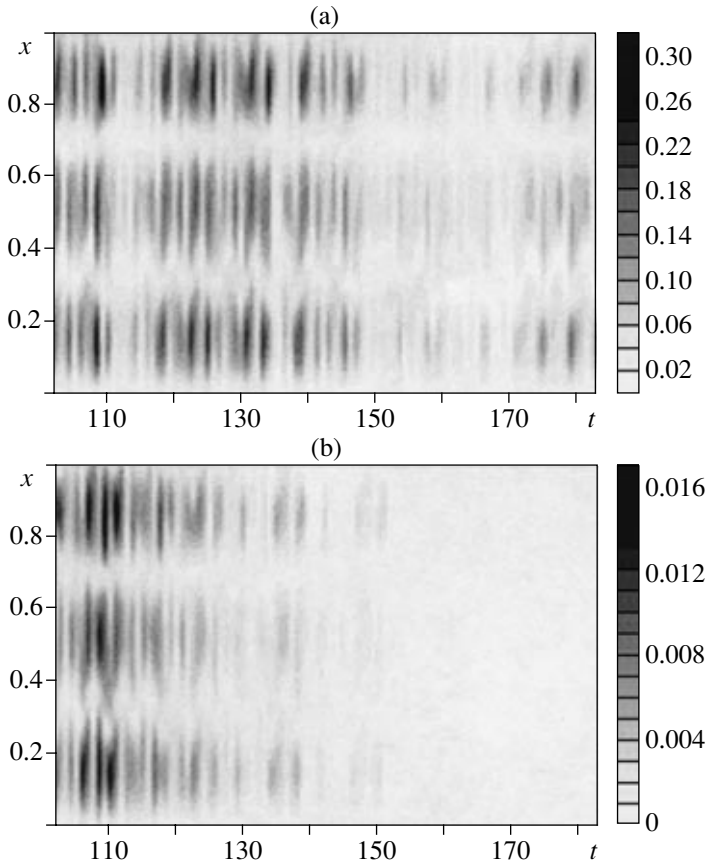

Fig. 4. Space–time evolution of the difference between the space-charge densities in the response and drive systems, $|\rho_2(x, t) - \rho_a(x, t)|$: (a) in the absence ($\varepsilon = 0.05$) and (b) in the presence ($\varepsilon = 0.2$) of the generalized synchronization mode: the space–time states of the response and drive systems are identical after the transient process.

become identical $\vec{x}_r(t) \equiv \vec{x}_a(t)$ after the end of a transient process. Thus, the equivalency of states of the response and auxiliary systems after the transient process (which may be considerably long [46]) is a criterion of generalized synchronization between the drive and response oscillators.

Another way to analyze the generalized synchronization mode is to use the method of conditional Lyapunov exponents. To this end, Lyapunov exponents are calculated for a nonautonomous response system. Since the behavior of the response system is dependent on that of the drive system, the calculated exponents are different than the Lyapunov exponents for the drive system and are referred to as conditional. In this case, unidirectionally coupled dynamic systems admit the generalized chaotic synchronization mode if the highest conditional Lyapunov exponent, λ, is negative [8, 45].

In order to use the auxiliary-system method to identify the generalized chaotic synchronization mode in the system of unidirectionally coupled Pierce diodes, the system of Eqs. (1)–(3) was solved for the auxiliary and response systems characterized by the same Pierce parameter but different initial conditions. To analyze the emergence of the generalized synchronization mode in the system, it is convenient to construct the difference of oscillations, $|\rho_2(x, t) - \rho_a(x, t)|$, in response system $\rho_2(x, t)$ and auxiliary system $\rho_a(x, t)$ and to consider this difference in the entire interaction space. The respective results are presented in Fig. 4, which indicates that, at a small coupling parameter, the oscillations of the charge density in the response and auxiliary systems remain different throughout the interaction space (Fig. 4a), while, at considerably high ε, these oscillations become identical (Fig. 4b); i.e., the mode of generalized chaotic synchronization is observed.

These results are confirmed by the calculation of the highest Lyapunov exponent, λ. Numerical calculation was accomplished via the method developed by Benettin and adapted for the analysis of a distributed system (see [43]). Figure 5 shows the corresponding typical dependence of the highest Lyapunov exponent on the coupling parameter for $\alpha_1 = 2.858\pi$ and $\alpha_2 = 2.862\pi$. It is seen that, at a certain value of the coupling parameter $\varepsilon = \varepsilon_{GS}$ (indicated by the arrow in Fig. 5), the highest Lyapunov exponent becomes negative and the generalized chaotic synchronization mode sets in.

By means of fixing the control parameter of one of the systems and varying the parameter of the other, it is possible to plot generalized synchronization threshold ε_{GS} as a function of the detuning between the subsystems. Figure 6a presents such a dependence for a fixed parameter of the drive system. It is seen that, as the parameter of the response system increases (the response system passes to simpler oscillation modes; see Fig. 1, which shows that, as α increases, the maximum Lyapunov exponent decreases and a transition from chaotic dynamics to regular oscillations takes place via a series of period doublings), the generalized synchronization threshold becomes lower.

Figure 6b plots threshold ε_{GS} at a fixed value of parameter α_2 of the response system and for different values of parameter α_1 of the drive system. One can see that, at small detunings between the drive and response systems, the generalized synchronization threshold depends only slightly on the parameters of the drive system. Thus, the distributed beam–plasma system passes to the generalized chaotic synchronization mode with an increase in the coupling parameter.

In our study [47], the modified-system method was used to reveal different mechanisms of setting generalized chaotic synchronization in systems with a small number of degrees of freedom. The idea of this method is to replace the system of two unidirectionally coupled chaotic oscillators with one modified response system operating under external action exerted by the drive system. This method helped to reveal the mechanisms of generalized synchronization that occur owing to an additional dissipation existing in a nonautonomous chaotic system in the generalized synchronization mode [47].

Let us apply the modified-system method to analyze the mechanism of generalized synchronization in coupled distributed beam–plasma systems. To do this, we require, in accordance with [47], that the dynamics of an autonomous modified response system be considered with allowance for unidirectional coupling introduced into the system. In our case, the autonomous modified distributed system is described by system (1)–(3) with the following boundary conditions for the potential:

$$\begin{aligned} \varphi_m(0, t) &= 0, \\ \varphi_m(1, t) &= -\varepsilon\rho_m(1, t)). \end{aligned} \tag{15}$$

Being written in this form, modified distributed system (1)–(3) can be considered in terms of the hydrodynamic model of a Pierce diode with an added feedback. A similar system was analyzed in more detail in [35, 36], where we considered the hydrodynamic model of a Pierce diode with an external feedback. It was shown that, with an increase in the feedback factor (parameter ε in the case under study), the hydrodynamic model passes from chaotic dynamics to periodic oscillations via a series of the period-doubling bifurcations.

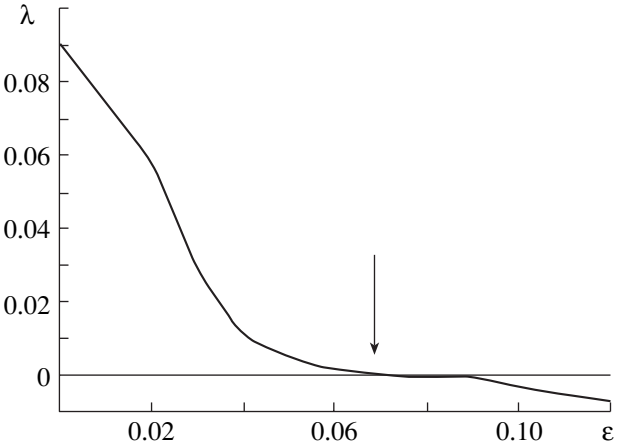

Fig. 5. Maximum conditional Lyapunov exponent vs. coupling parameter ε for the Pierce parameters of the response and drive systems, $\alpha_1 = 2.858\pi$ and $\alpha_2 = 2.862\pi$. The arrow points to the coupling parameter at which the system passes to the generalized synchronization mode (the maximum Lyapunov exponent becomes negative).

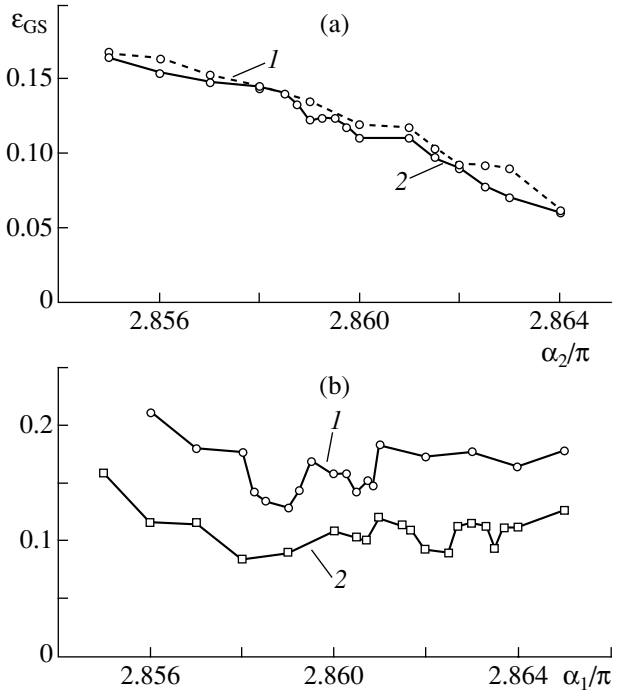

Fig. 6. Threshold of the generalized synchronization mode vs. Pierce parameters (a) α_1 of the drive system and (b) α_2 of the response system. (The Pierce parameter of the other system is fixed at 2.859π for curve *1* and 2.862π for curve *2*.)

As was shown in [47], the necessary condition for the emergence of the generalized synchronization mode is the possibility for regular oscillations or stationary states to arise in the modified system with an increase in the value of coupling parameter ε. Therefore, taking into account the results of [35, 36], one can argue that the mechanism underlying the generalized

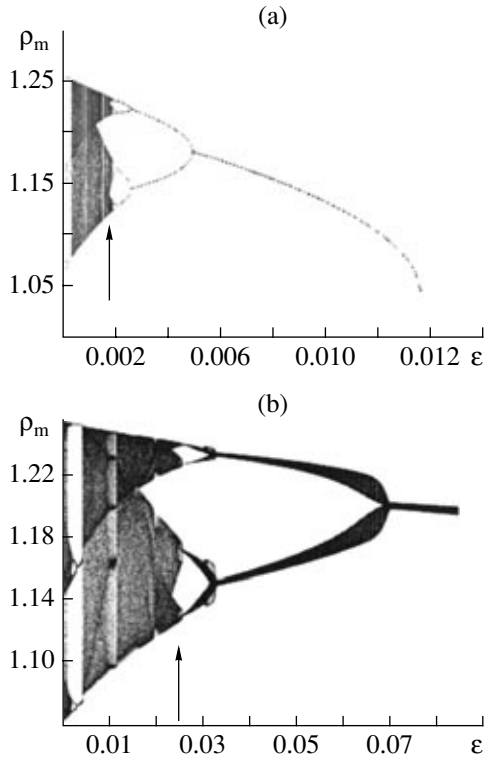

Fig. 7. Bifurcation diagrams of the space-charge density oscillations in the modified system with the parameter $\alpha_m = 2.862\pi$ (a) in the case of autonomous dynamics and (b) under a harmonic external action.

synchronization mode in the hydrodynamic model of a Pierce diode is the mechanism discovered in [47]. However, in the case under study, this mechanism is determined by the rearrangement of oscillation modes that occurs owing to the feedback introduced into the system, rather than by introduction of extra dissipation into the system.

The above considerations are illustrated by Fig. 7, which shows the bifurcation diagram for oscillations of the space-charge density in a Pierce diode with a feedback (recorded at point $x = 0.2$ of the interaction space) with ε taken as the varied parameter. The diagram shows that, with an increase in the coupling parameter, oscillations in the modified system become periodic and, then, a stationary state sets in. However, the coupling parameter at which the oscillations become periodic is much lower than generalized synchronization threshold ε_{GS}. The reason for this circumstance is that, in order to find the generalized synchronization threshold, one should consider a modified system under external action, as discussed in [47]. In this case, the external action increases the value of parameter ε at which oscillations become periodic. Such behavior can be clarified through consideration of the dynamics of the modified system under an external periodic action. In the simplest case, such an external action may be taken as harmonic, while the frequency and amplitude must correspond to the fundamental frequency in the power spectrum of the drive chaotic system.

In this case, boundary conditions (15) for modified system (1)–(3) should be modified by addition of the external harmonic signal:

$$\begin{aligned} \varphi_m(0, t) &= 0, \\ \varphi_m(1, t) &= -\varepsilon\rho_r(1, t) + \varepsilon A\cos(2\pi f_0 t), \end{aligned} \tag{16}$$

where $A = 0.8$ and $f_0 = 1.0$ are chosen so as to model the main peak in the power spectrum of the drive system.

The corresponding bifurcation diagram for oscillations in the Pierce diode is shown in Fig. 7b. The bifurcation points for the modified system with the external action are seen to shift toward larger ε with respect to the autonomous case (Fig. 7a). At the same time, the diagram shows that, at high values of coupling ε, oscillations are not periodic but dual-frequency with incommensurable time scales (quasi-periodic regular oscillations). Therefore, the generalized synchronization threshold is higher than the value of parameter ε at which the autonomous modified system passes from chaotic oscillations to periodic dynamics.

CONCLUSIONS

For the first time, various types of chaotic synchronization (complete synchronization and time-scale synchronization) have been shown to be feasible in a system of coupled beam–plasma subsystems with supercritical current (coupled hydrodynamic models of Pierce diodes). A new approach to the analysis of chaotic synchronization—time scale synchronization—has been applied [16–18]. Of special note is the possibility of complete synchronization of chaotic space–time beam–plasma oscillations, a circumstance that makes such self-oscillating systems applicable for data transmission in the microwave frequency band [26].

In the case of unidirectional coupling, an increase in the coupling parameter results in transition from asynchronous behavior to the generalized synchronization mode. At a fixed value of the control parameter (the Pierce parameter) of the drive system, the generalized synchronization threshold decreases with an increase in the Pierce parameter of the response system. If the Pierce parameter of the response system is constant, the generalized synchronization threshold shows only a weak dependence on the Pierce parameters of the drive system. Such behavior of the generalized synchronization threshold has been explained via the modified-system method, which was proposed for analysis of the generalized synchronization of lumped systems in [47].

ACKNOWLEDGMENTS

This study was supported by the Russian Foundation for Basic Research (project nos. 05-02-16286, 06-02-81013, and 07-02-00044).

We thank the Dynasty Foundation and the International Center for Basic Physics (Moscow) for financial support.

REFERENCES

1. S. Boccaletti, J. Kuths, G. Osipov, et al., Phys. Rep. **366**, 1 (2002).
2. A. Pikovskii, M. Rozenblyum, and J. Kurths, *Synchronization. A Fundamental Nonlinear Phenomenon* (Tekhnosfera, Moscow, 2003) [in Russian].
3. V. S. Anishchenko, V. V. Astakhov, T. E. Vadivasova, et al., *Nonlinear Effects in Chaotic Stochastic Systems* (Inst. Kosm. Issled., Izhevsk–Moscow, 2003) [in Russian].
4. I. Z. Kiss, J. L. Hudson, J. Escalona, and P. Parmananda, Phys. Rev. E **70**, 026210 (2004).
5. L. Glass, Nature (London) **410**, 277 (2001).
6. E. Mosekilde, Yu. Maistrenko, and D. Postnov, in *Chaotic Synchronization, Applications To Living Systems* (World Sci., Singapore, 2002), Ser. A., Vol. 42.
7. M. G. Rosenblum, A. S. Pikovsky, and J. Kurths, Phys. Rev. Lett. **76**, 1804 (1996).
8. K. Pyragas, Phys. Rev. E **54**, R4508 (1996).
9. H. D. I. Abarbanel, N. F. Rullkov, and M. M. Sushchik, Phys. Rev. E **53**, 4528 (1996).
10. M. G. Rosenblum, A. S. Pikovsky, and J. Kurths, Phys. Rev. Lett. **78**, 4193 (1997).
11. A. Pikovsky, M. Rosenblum, and J. Kurths, Int. J. Bifurcation and Chaos **10**, 2291 (2000).
12. A. E. Hramov, A. A. Koronovskii, M. K. Kurovskaya, and O. I. Moskalenko, Phys. Rev. E **71**, 056204 (2005).
13. N. F. Rulkov, M. M. Sushchik, L. S. Tsimring, and H. D. I. Abarbanel, Phys. Rev. E **51**, 980 (1995).
14. L. M. Pecora, T. L. Carroll, G. A. Jonson, and D. J. Mar, Chaos **7**, 520 (1997).
15. A. A. Koronovskii and A. E. Hramov, Pis'ma Zh. Eksp. Teor. Fiz. **79**, 391 (2004) [JETP Lett. **79**, 316 (2004)].
16. A. E. Hramov and A. A. Koronovskii, Chaos **14**, 603 (2004).
17. A. E. Hramov and A. A. Koronovskii, Phys. D (Amsterdam) **206** (3–4), 252 (2005).
18. A. E. Hramov, A. A. Koronovskii, and Yu. I. Levin, Zh. Eksp. Teor. Fiz. **127**, 886 (2005) [JETP **100**, 784 (2005)].
19. A. A. Koronovskii and A. E. Hramov, *Continuous Wavelet Analysis and Its Applications* (Fizmatlit, Moscow, 2003) [in Russian].
20. A. A. Koronovskii, O. I. Moskalenko, and A. E. Hramov, Pis'ma Zh. Eksp. Teor. Fiz. **80**, 25 (2004) [JETP Lett. **80**, 20 (2004)].
21. V. S. Afraimovich, V. I. Nekorkin, G. V. Osipov, and V. D. Shalfeev, *Stability, Structures, and Chaos in Nonlinear Synchronization Networks*, Ed. by A. V. Gaponov-Grekhov and M. I. Rabinovich (IPF AN SSSR, Gorki, 1989) [in Russian].
22. L. Kocarev, Z. Tasev, T. Stojanovski, and U. Parlitz, Chaos **7**, 635 (1997).
23. S. Boccaletti, J. Bragard, F. T. Arecchi, and H. Mancini, Phys. Rev. Lett. **83**, 536 (1999).
24. Z. Tasev, L. Kocarev, L. Junge, and U. Parlitz, Int. J. Bifurcation and Chaos **10**, 869 (2000).
25. E. Rosa, W. Pardo, and C. Ticos, Int. J. Bifurcation and Chaos **10**, 2551 (2000).
26. A. S. Dmitriev and A. I. Panas, *Dynamic Chaos: New Information Carriers for Communications Systems* (Fizmatlit, Moscow, 2002) [in Russian].
27. A. E. Hramov, A. A. Koronovskii, P. V. Popov, and I. S. Rempen, Chaos **15**, 013705 (2005).
28. A. A. Koronovskii, P. V. Popov, and A. E. Hramov, Zh. Tekh. Fiz. **75** (4), 1 (2005) [Tech. Phys. **75**, 385 (2005)].
29. D. I. Trubetskov and A. E. Hramov, *Lectures on Microwave Electronics for Physicists* (Fizmatlit, Moscow, 2003), Vol. 1 [in Russian].
30. B. B. Godfrey, Phys. Fluids **30**, 1553 (1987).
31. S. Kuhn and A. Ender, J. Appl. Phys. **68**, 732 (1990).
32. V. G. Anfinogentov and D. I. Trubetskov, Radiotekh. Elektron. (Moscow) **37**, 2251 (1992).
33. H. Matsumoto, H. Yokoyama, and D. Summers, Phys. Plasmas **3**, 177 (1996).
34. T. Klinger, C. Schroder, D. Block, et al., Phys. Plasmas **8**, 1961 (2001).
35. A. E. Hramov and I. S. Rempen, Radiotekh. Elektron. (Moscow) **47**, 732 (2002) [J. Commun. Technol. Electron. **47**, 658 (2002)].
36. A. E. Hramov and I. S. Remplen, Int. J. Electron. **91** (1), 11 (2004).
37. Yu. A. Kalinin, A. A. Koronovskii, A. E. Hramov, et al., Fiz. Plazmy **31**, 1009 (2005) [Plasma Phys. Rep. **31**, 938 (2005)].
38. M. V. Kuzelev and A. A. Rukhadze, Electrodynamics of Dense Electron Beams in Plasma (Nauka, Moscow, 1990) [in Russian].
39. M. V. Kuzelev, A. A. Rukhadze, and P. S. Strelkov, *Relativistic Microwave Plasma Electronics* (MGTU, Moscow, 2002) [in Russian].
40. J. Pierce, J. Appl. Phys. **15**, 721 (1944).
41. Yu. A. Kalinin and A. D. Esin, *Methods and Facilities of Physical Experiment in Vacuum Microwave Electronics* (Saratov. Gos. Univ., Saratov, 1991) [in Russian].
42. P. J. Roach, *Computational Fluid Dynamics* (Hermosa, Albuquerque, 1976; Mir, Moscow, 1980).
43. A. A. Koronovskii, I. S. Rempen, and A. E. Hramov, Izv. Akad. Nauk, Ser. Fiz. **67**, 1708 (2003).
44. J. Bragard, F. T. Arecchi, and S. Boccaletti, Int. J. Bifurcation and Chaos **10**, 2381 (2000).
45. L. M. Pecora and T. L. Carroll, Phys. Rev. A **44**, 2374 (1991).
46. A. E. Hramov and A. A. Koronovskii, Europhys. Lett. **70** (2), 169 (2005).
47. A. E. Hramov and A. A. Koronovskii, Phys. Rev. **71**, 067201 (2005).